European Conference on Computational Fluid Dynamics
ECCOMAS CFD 2006
P. Wesseling, E. Oñate and J. Périaux (Eds)

REGULARIZATION MODELING FOR LARGE-EDDY SIMULATION OF DIFFUSION FLAMES

Bernard J. Geurts[1,2]

[1] Multiscale Modeling and Simulation, NACM, J.M. Burgers Center, Faculty EEMCS, University of Twente, P.O. Box 217, 7500 AE Enschede, the Netherlands
[2] Anisotropic Turbulence, Fluid Dynamics Laboratory, Department of Applied Physics, Eindhoven University of Technology, P.O. Box 513, 5300 MB Eindhoven, the Netherlands
e-mail: b.j.geurts@utwente.nl

Key words: turbulence, combustion, large-eddy simulation, regularization modeling, iso-surface analysis

Abstract. *We analyze the evolution of a diffusion flame in a turbulent mixing layer using large-eddy simulation. The large-eddy simulation includes Leray regularization of the convective transport and approximate inverse filtering to represent the chemical source terms. The Leray model is compared to the more conventional dynamic mixed model. The location of the flame-center is defined by the 'stoichiometric' interface. Geometrical properties such as its surface-area and wrinkling are characterized using an accurate numerical level-set quadrature method. This allows to quantify flame-properties as well as turbulence modulation effects due to coupling between combustion and turbulent transport. We determine the active flame-region that is responsible for the main part of the chemical conversion in the flame and compare direct and large-eddy simulation predictions.*

1 Introduction

In various combustion processes turbulent diffusion flames arise. These are characterized by a thin, distorted and lively evolving region where the conditions for combustion, such as presence of chemical species at appropriate concentration and temperature, are fulfilled [1]. We will consider combustion in a turbulent mixing layer with stylized chemical reaction process [2]. This computational model can be treated in full detail and provides an impression of the dominant turbulence modulation that arises from the coupling between the fluid-flow and the chemical reaction equations.

It is the purpose of this paper to analyze the capabilities of large-eddy simulation of diffusion flames. This requires a proper capturing of the three central closure problems, i.e., for *(i)* the turbulent stresses, *(ii)* the velocity-species correlations and *(iii)* the chemical source terms. We will focus on a comparison between Leray regularization [3, 4] and dynamic mixed modeling [5, 6] for the turbulent stresses. These types of modeling may also be adopted to express the velocity-species correlations. In addition, we will

consider an inverse modeling [7, 8] of the chemical source terms. Specifically, the filtered nonlinear source terms are formulated in 'reconstructed' flow variables. This requires the application of an approximate inversion of the spatial large-eddy filter.

The central region of a diffusion flame may be visualized by monitoring the so-called 'stoichiometric' interface. In a turbulent flow this interface develops into a complex, highly wrinkled surface. Fundamental properties such as the flame's surface-area and its wrinkling can be appreciated roughly by visual inspection. However, a more meaningful assessment can be obtained from a quantitative analysis of the flame surface. Access to these fundamental flame-properties can be used as under-pinning of theoretical and modeling studies. Moreover, a better understanding of the combustion process is basic to refined control technology aimed at combustion with minimal generation of pollutant [9]. Questions concerning the quality with which the dynamics of the turbulent flame may be predicted by large-eddy simulation provide the focus of this paper.

Compared to the dynamic mixed modeling, the regularization modeling of the turbulent stresses will be shown to better retain the small-scale variability of a turbulent flow. To illustrate this, the mixing-rate and the kinetic energy spectrum are determined under combustion conditions. The regularization and dynamic mixed models properly capture the reduced mixing at high heat-release. The Leray model predicts a significantly higher tail of the kinetic energy spectrum compared to the dynamic mixed model. This also affects important global flame-properties such as the evolving surface-area and wrinkling of the flame as will be quantified using a level-set analysis [10].

The organization of this paper is as follows. In section 2 we will introduce the computational model used to describe a diffusion flame in a temporal mixing layer. Section 3 is devoted to the introduction of the large-eddy formulation, both for the turbulent flow as well as for the combustion model. The prediction of the reduced mixing-rate and kinetic energy spectrum, under intense combustion conditions, will be considered in section 4. Section 5 is devoted to a description and application of the method of iso-surface analysis of the flame. Specifically, the determination of the 'active flame region' is discussed. Finally, in section 6 some concluding remarks are collected.

2 Diffusion flame in a mixing layer

In this section we will introduce the mathematical model describing the flame problem studied in this paper. Subsequently, we will introduce the temporal mixing layer [11] and visualize the evolution of the flame.

2.1 Mathematical model of simplified combustion

The computational model is composed of the compressible flow equations for ideal gases, coupled to a system of advection-diffusion-reaction equations [9, 12]. The dimensionless system of equations that is considered here can be expressed in three dimensions

as

$$\partial_t \rho + \partial_j(\rho u_j) = 0 \tag{1}$$
$$\partial_t(\rho u_i) + \partial_j(\rho u_i u_j) + \partial_i p - \partial_j \sigma_{ij} = 0 \quad ; \quad i = 1, \ldots, 3 \tag{2}$$
$$\partial_t e + \partial_j((e+p)u_j) - \partial_j(\sigma_{ij} u_i) + \partial_j q_j - h_k \omega_k = 0 \tag{3}$$
$$\partial_t(\rho c_k) + \partial_j(\rho c_k u_j) - \partial_j(\pi_{kj}) - \omega_k = 0 \quad ; \quad k = 1, \ldots, N_s \tag{4}$$

where ρ denotes the fluid mass-density, u_i the velocity in the x_i direction, e the total energy density and c_k the k-th chemical species concentration. We consider N_s different species. Partial derivatives with respect to time t and spatial coordinate x_i are denoted by ∂_t and ∂_i respectively. Summation over repeated indices is implied. The continuity equation (1) represents conservation of mass. The conservation principles for momentum and energy are contained in (2) and (3). The latter equation contains in addition contributions from heat released by the chemical processes. Finally, the conservation principle for the individual species is provided in (4).

In order to close this system of equations, additional constitutive relations need to be provided. We follow the standard description given in [12] in which:

- The viscous fluxes are specified by $\pi_{kj} = \partial_j c_k/(Re\, Sc)$ and $\sigma_{ij}(\mathbf{u}) = S_{ij}/Re$, with rate of strain tensor given by

$$S_{ij} = \partial_i u_j + \partial_j u_i - \frac{2}{3}\delta_{ij}\partial_k u_k \tag{5}$$

  The Reynolds (Re) and Schmidt (Sc) numbers characterize the strength of the viscous fluxes relative to the nonlinear convective contributions in the momentum and species equations. Throughout we will adopt $Sc = 10$.

- The equation of state for an ideal gas specifies the pressure p through

$$e = \frac{p}{\gamma - 1} + \frac{1}{2}\rho u_i u_i \tag{6}$$

  where the adiabatic constant $\gamma \approx 7/5$.

- The heat flux vector is given by

$$q_j = -\frac{\partial_j T}{(\gamma - 1) Re Pr M^2} \tag{7}$$

  where Pr is the Prandtl number, M the Mach number and the temperature T follows from the ideal gas law $\rho T = \gamma M^2 p$. Throughout we put $Pr = 1$ and $M = 0.2$.

The chemical reactions associated with the combustion are described by source terms in the energy equation (3) and the species equations (4). We turn to this part of the computational model next.

A large class of chemical reactions may be expressed in terms of a multi-species, multi-step process [13]. In general, the N_s chemical species may be involved in N_c chemical reactions. Let $\mathcal{M}_i$ denote the chemical species and $\nu^r_{i,l}$, $\nu^p_{i,l}$ the stoichiometric coefficients of the i-th species, viewed as reactants (r) and products (p) in the l-th reaction, respectively. The multi-species, multi-step chemical reaction involves transitions that may be expressed as:

$$\nu^r_{i,l}\mathcal{M}_i \rightarrow \nu^p_{i,l}\mathcal{M}_i \quad ; \quad l = 1, \ldots, N_c \tag{8}$$

This describes the l-th reaction in which $\nu^r_{i,l}$ 'units' of species $\mathcal{M}_i$, $i = 1, \ldots, N_s$ give rise to $\nu^p_{i,l}$ units after the reaction. We will consider only a single, very simple reaction in which a fuel F reacts with an oxidizer O to yield a product P:

$$F + O \rightarrow P \tag{9}$$

This particular combustion model involves $N_s = 3$ species in $N_c = 1$ reaction in which $\nu^r_F = \nu^r_O = 1$ units of fuel and oxidizer combine into $\nu^p_P = 1$ units of product. In this stylized description fuel and oxidizer are lost after the reaction, i.e., $\nu^p_F = \nu^p_O = 0$ while there was no product ahead of the reaction, i.e., $\nu^r_P = 0$. In the sequel we associate F with species 1, O with species 2 and P with species 3.

The chemical reaction rate ω_i is assumed to be determined by the Arrhenius law [1]:

$$\frac{\omega_i}{W_i} = (\nu^p_{i,l} - \nu^r_{i,l}) Da_l \exp(-\frac{Ze_l}{T}) \prod_{k=1}^{N_s} \Big(\frac{\rho c_k}{W_k}\Big)^{\nu^r_{k,l}} \quad ; \quad i = 1, \ldots, N_s \tag{10}$$

where summation over l is implied and W_i is the molecular weight of species $\mathcal{M}_i$. Moreover, Da_l and Ze_l denote the Damköhler and Zeldovich numbers respectively of the l-th reaction. For the particular reaction $F + O \rightarrow P$ we can simplify the expressions for the reaction-rates further and obtain:

$$\omega_1 = -(\rho c_F)(\rho c_O)\frac{Da}{W_O}\exp(-\frac{Ze}{T}) \tag{11}$$

$$\omega_2 = -(\rho c_F)(\rho c_O)\frac{Da}{W_F}\exp(-\frac{Ze}{T}) \tag{12}$$

$$\omega_3 = (\rho c_F)(\rho c_O)\frac{DaW_P}{W_F W_O}\exp(-\frac{Ze}{T}) \tag{13}$$

Since $W_P = W_F + W_O$ we may write

$$\frac{DaW_P}{W_F W_O} = \frac{Da(W_F + W_O)}{W_F W_O} = \frac{Da}{W_O}\Big(1 + \frac{W_O}{W_F}\Big) = Da_O(1 + \alpha) \tag{14}$$

where we introduced the 'compensated' Damköhler number $Da_O = Da/W_O$ and the weight-ratio $\alpha = W_O/W_F$. Correspondingly, we infer

$$\omega_1 = -(\rho c_F)(\rho c_O) Da_O \exp(-\frac{Ze}{T}) \;\; ; \;\; \omega_2 = \alpha\omega_1 \;\; ; \;\; \omega_3 = -(1+\alpha)\omega_1 \tag{15}$$

The source term in the energy equation can be expressed as

$$\begin{aligned} h_j\omega_j &= h_1\omega_1 + h_2\omega_2 + h_3\omega_3 = h_1\omega_1 + \alpha h_2\omega_1 - (1+\alpha)h_3\omega_1 \\ &= \omega_1(h_1 + \alpha h_2 - (1+\alpha)h_3) = Q\omega_1 \end{aligned} \tag{16}$$

where the individual enthalpies are denoted by h_j and Q will be referred to as the effective standard enthalpy of formation. In total the combustion model requires the evaluation of ω_1 and four additional parameters: Da_O, Ze, Q and α. Throughout we will adopt $Da_O = 1$, $Ze = 1$ and $\alpha = 1$ and focus on effects arising from variations in Q. The validity of these parameter-values in real combustion processes needs to be investigated to improve the physical understanding of the observed phenomena. This requires an extensive parameter-study which is subject of ongoing research.

2.2 Numerical method for diffusion flame

We simulate the compressible three-dimensional temporal mixing layer and use a Reynolds number based on the upper stream velocity and half the initial vorticity thickness of 50 [11]. The governing equations are solved in a cubic geometry of side ℓ which is set equal to four times the wavelength of the most unstable mode according to linear stability theory, i.e., under the chosen conditions $\ell = 59$. Periodic boundary conditions are imposed in the streamwise (x_1) and spanwise (x_3) direction, while in the normal (x_2) direction the boundaries are free-slip walls. The initial condition is formed by mean profiles corresponding to constant pressure $p = 1/(\gamma M^2)$, $u_1 = \tanh(x_2)$ for the streamwise velocity component, $u_2 = u_3 = 0$ and a temperature profile given by the Busemann-Crocco law. Superimposed on the mean profile are two- and three-dimensional perturbation modes obtained from linear stability theory.

We use explicit time-integration with a second order, compact storage, four-stage Runge-Kutta scheme. A fourth order accurate spatial discretization method is adopted for the convective fluxes while a second order central finite volume scheme is used for the viscous fluxes. The treatment of the convective fluxes adopts, e.g., for the derivative of a field f with respect to x_1 [12]

$$\begin{aligned} (\delta_1 f)_{i,j,k} &= (-s_{i+2,j,k} + 8s_{i+1,j,k} - 8s_{i-1,j,k} + s_{i-2,j,k})/(12\Delta x_1) \\ s_{i,j,k} &= (-g_{i,j-2,k} + 4g_{i,j-1,k} + 10g_{i,j,k} + 4g_{i,j+1,k} - g_{i,j+2,k})/16 \\ g_{i,j,k} &= (-f_{i,j,k-2} + 4f_{i,j,k-1} + 10f_{i,j,k} + 4f_{i,j,k+1} - f_{i,j,k+2})/16 \end{aligned} \tag{17}$$

in which Δx_1 is the grid-spacing in the x_1-direction. This scheme is conservative and the coefficients in the definition for $g_{i,j,k}$ are chosen such that $g_{i,j,k}$ is a fourth order accurate

approximation to $f_{i,j,k}$ while small-scale 'numerical' grid-oscillations in the x_3-direction give no contributions to $g_{i,j,k}$. The definition for $s_{i,j,k}$ has the same properties with respect to the x_2-direction. The viscous terms contain second-order derivatives which are treated by a consecutive application of two first order numerical derivatives. This requires for example that the gradient of the velocity is calculated in centers of grid-cells. In center $(i+\frac{1}{2}, j+\frac{1}{2}, k+\frac{1}{2})$ the corresponding discretization $D_1 f$ has the form

$$\begin{aligned} (D_1 f)_{i+\frac{1}{2},j+\frac{1}{2},k+\frac{1}{2}} &= (s_{i+1,j+\frac{1}{2},k+\frac{1}{2}} - s_{i,j+\frac{1}{2},k+\frac{1}{2}})/\Delta x_1 \\ \text{with} \quad s_{i,j+\frac{1}{2},k+\frac{1}{2}} &= (f_{i,j,k} + f_{i,j+1,k} + f_{i,j,k+1} + f_{i,j+1,k+1})/4 \end{aligned} \tag{18}$$

The second derivative is subsequently calculated in the point (i, j, k) by applying the operator D_1 again, but now to the staggered approximations of the first derivative [4]. The basic numerical method thus consists of explicit second order accurate four-stage Runge-Kutta time-stepping, fourth order accurate treatment of the convective fluxes and second order finite volume discretization for the viscous contributions.

Visualization of the flow under conditions studied here demonstrates the roll-up of the fundamental instability. Four rollers with mainly negative spanwise vorticity develop. These undergo two distinct pairings. After the first pairing the flow has become highly three-dimensional. Another pairing yields a single roller in which the flow exhibits a complex structure, with many regions of positive spanwise vorticity.

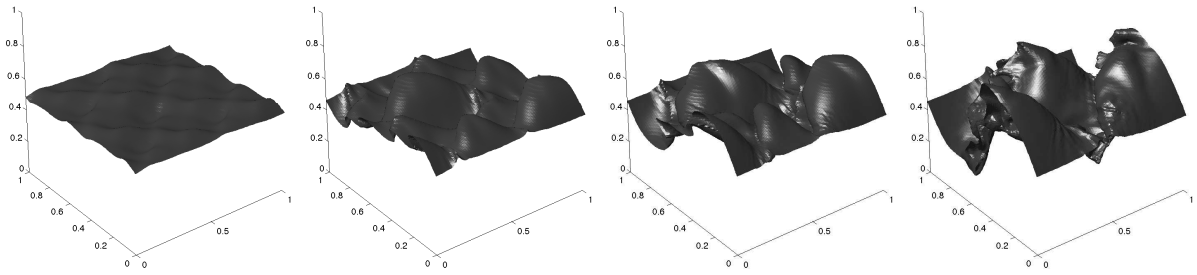

Figure 1: Evolving stoichiometric surface $c_F - c_O = 0$ in a turbulent mixing layer, using $Da = 1$, $Ze = 1$, $\alpha = 1$ and a heat-release $Q = -1$. The snapshots are taken at $t = 15, 35, 55, 75$ (from left to right).

The consequences of combustion for turbulence dynamics may be investigated within the basic temporal mixing layer configuration. In this paper we consider initially the upper stream to contain fuel ($c_F = 1, c_O = 0$) and the lower stream to contain oxidizer ($c_O = 1, c_F = 0$). The initial condition is assumed to contain no 'product' ($c_P = 0$). The 'center' of the flame is defined through the 'stoichiometric surface' where $c_F - c_O = 0$. The evolution of this level-set is shown in figure 1. This result was obtained from a direct numerical simulation using 192^3 grid-cells [11] which provides a good qualitative illustration of the wrinkled shape of the flame. A more quantitative analysis will be presented momentarily.

3 Large-eddy modeling of diffusion flames

In this section we present the large-eddy formulation and corresponding subgrid modeling in subsection 3.1. The inverse modeling of the chemical source terms will be described in subsection 3.2.

3.1 Spatial filtering and subgrid closure

In the filtering approach to large-eddy simulation, a spatial convolution filter is applied to the governing equations given by (1)-(4). Specifically, we introduce the filtered field $\overline{f}$ associated with an unfiltered field f through

$$\overline{f}(\mathbf{x},t) = L(f) = \int_{-\infty}^{\infty} G(\mathbf{x}-\boldsymbol{\xi})u(\boldsymbol{\xi},t)\; d\boldsymbol{\xi} \tag{19}$$

where the filter-kernel G has a width Δ and we assume $G(\mathbf{z}) = G_1(z_1)G_2(z_2)G_3(z_3)$, i.e., the product of three filter-kernels associated with filtering in the x_1, x_2 and x_3 directions respectively. We assume that the filter L is normalized. Next to this basic filter, it is convenient to define the corresponding Favre filter in which

$$\widetilde{f} = \frac{\overline{\rho f}}{\overline{\rho}} = \frac{L(\rho f)}{L(\rho)} = L_\rho(f) \tag{20}$$

in terms of the Favre operator L_ρ.

Application of the spatial filter L to (1)-(4) results in the following system of equations:

$$\partial_t\overline{\rho} + \partial_j(\overline{\rho}\widetilde{u}_j) = 0 \tag{21}$$
$$\partial_t(\overline{\rho}\widetilde{u}_i) + \partial_j(\overline{\rho}\widetilde{u}_i\widetilde{u}_j) + \partial_i\overline{p} - \partial_j\breve{\sigma}_{ij} = -\partial(\overline{\rho}\tau_{ij}) + \partial_j(\overline{\sigma}_{ij} - \breve{\sigma}_{ij}) \tag{22}$$
$$\partial_t\breve{e} + \partial_j((\breve{e}+\overline{p})\widetilde{u}_j) - \partial_j(\breve{\sigma}_{ij}\widetilde{u}_i) + \partial_j\breve{q}_j = \mathcal{A} + \overline{h_k\omega_k} \tag{23}$$
$$\partial_t(\overline{\rho}\widetilde{c}_k) + \partial_j(\overline{\rho}\widetilde{c}_k\widetilde{u}_j) - \partial_j(\breve{\pi}_{kj}) = -\partial_j(\overline{\rho}\zeta_{jk}) + \partial(\overline{\pi}_{kj} - \breve{\pi}_{kj}) + \overline{\omega}_k \tag{24}$$

in terms of the filtered variables $\overline{\rho}$, $\widetilde{u}_j$, $\overline{p}$ and $\widetilde{c}_k$. In these equations we denote the smoothed viscous flux by $\breve{\sigma}_{ij} = \sigma_{ij}(\widetilde{\mathbf{u}})$ and obtain the smoothed energy and heat flux through

$$\breve{e} \;=\; \frac{\overline{p}}{(\gamma-1)} + \frac{1}{2}\widetilde{u}_i\widetilde{u}_i \tag{25}$$

$$\breve{q}_j \;=\; -\frac{\partial_j\widetilde{T}}{(\gamma-1)RePrM^2} \tag{26}$$

in which $\widetilde{T} = \gamma M^2\overline{p}/\overline{\rho}$. Moreover, the smoothed viscous fluxes in the species equations are given by $\breve{\pi}_{kj} = \partial_j\widetilde{c}_k/(ReSc)$. Apart from these contributions in terms of the filtered variables a number of additional contributions arises which constitute the combined closure problem:

- *Turbulent stress tensor:* The filtered nonlinear convective flux may be expressed as

$$\partial_j(\overline{\rho u_i u_j}) = \partial_j(\overline{\rho}\widetilde{u}_i\widetilde{u}_j) + \partial(\overline{\rho}\Big(\widetilde{u_i u_j} - \widetilde{u}_i\widetilde{u}_j\Big)) = \partial_j(\overline{\rho}\widetilde{u}_i\widetilde{u}_j) + \partial(\overline{\rho}\tau_{ij}) \tag{27}$$

  in which the turbulent stress tensor is given by

$$\tau_{ij} = \widetilde{u_i u_j} - \widetilde{u}_i\widetilde{u}_j = L_\rho(u_i u_j) - L_\rho(u_i)L_\rho(u_j) = \Big[L_\rho, \Pi\Big](u_i, u_j) \tag{28}$$

  In this expression τ_{ij} is written in terms of the commutator of the Favre filtering L_ρ and the product-operator $\Pi(f,g) = fg$.

- *Velocity-species stress tensor:* The filtering of the advection term in the species equations implies

$$\partial_j(\overline{\rho u_j c_k}) = \partial(\overline{\rho}\widetilde{u}_j\widetilde{c}_k) + \partial(\overline{\rho}\zeta_{jk}) \tag{29}$$

  where we put

$$\zeta_{jk} = \widetilde{u_j c_k} - \widetilde{u}_j\widetilde{c}_k = [L_\rho, \Pi](u_j, c_k) \tag{30}$$

- *Energy equation closure terms:* filtering the energy equation gives rise to a large number of subgrid terms. These are summarized in the symbol $\mathcal{A}$. At low Mach number M the contributions of these closure terms can be neglected [14]. We restrict to such cases in the sequel, i.e., assume $\mathcal{A} \approx 0$.

- *Viscous closure fluxes:* Terms such as $\overline{\sigma}_{ij} - \breve{\sigma}_{ij}$ and $\overline{\pi}_{kj} - \breve{\pi}_{kj}$ arise from the difference between the Favre (L_ρ) and the basic filter (L). In case compressibility effects are small these terms can be neglected. We will restrict to such conditions here.

The filtered source terms $\overline{\omega}_k$ in (24) and the filtered heat-release term $\overline{h_k\omega_k}$ in (23) also need to be accounted for in the smoothed compressible equations. We discuss the modeling of these chemical source terms in subsection 3.2 and next turn to the closure of the filtered convective terms, expressed by τ_{ij} and ζ_{jk}.

A variety of subgrid models has been proposed for the turbulent stress tensor. In this paper we will compare dynamic mixed modeling [6] with Leray regularization [3]. For notational convenience we present these models in their incompressible formulation. In actual simulations the compressible implementation is adopted.

The mixed model combines Bardina's similarity model [15] with Smagorinsky's eddy-viscosity model [16]: $\tau_{ij} \rightarrow m_{ij}^M = m_{ij}^B - C_d\Delta^2|S|S_{ij}$. Here C_d denotes the dynamic coefficient and the similarity model is given by $m_{ij}^B = [L,\Pi](\overline{u}_i, \overline{u}_j)$. The dynamic coefficient is determined in accordance with the evolving flow, starting from Germano's identity [17, 18]:

$$T_{ij} - \widehat{\tau_{ij}} = R_{ij} \tag{31}$$

where

$$T_{ij} = \widehat{\overline{u_i u_j}} - \widehat{\overline{u}}_i\widehat{\overline{u}}_j \quad \text{and} \quad R_{ij} = \widehat{(\overline{u}_i\overline{u}_j)} - \widehat{\overline{u}}_i\widehat{\overline{u}}_j \tag{32}$$

In this two-level identity a so-called explicit test filter $\widehat{(\cdot)}$ is introduced. The implementation of the dynamic procedure starts by assuming the mixed model $m_{ij} = a_{ij}(\overline{\mathbf{u}}) + cb_{ij}(\overline{\mathbf{u}})$ for τ_{ij} and $M_{ij} = A_{ij} + CB_{ij}$ for T_{ij} where $A_{ij} = a_{ij}(\widehat{\overline{\mathbf{u}}})$, $B_{ij} = b_{ij}(\widehat{\overline{\mathbf{u}}})$. The assumption $C \approx c$ is invoked and we introduce the notations $\mathcal{A}_{ij} = A_{ij} - \widehat{a}_{ij}$, $\mathcal{B}_{ij} = B_{ij} - \widehat{b}_{ij}$. If we use the approximation $\widehat{(cb_{ij})} \approx c(\widehat{b}_{ij})$, insertion in Germano's identity yields $\mathcal{A}_{ij} + c\mathcal{B}_{ij} = R_{ij}$. This relation should hold for all tensor-components individually. However, only a single scalar field c is introduced in this model. Therefore, a least squares formulation is adopted from which we find [19]

$$c = \frac{\langle (R_{ij} - \mathcal{A}_{ij})\mathcal{B}_{ij} \rangle}{\langle \mathcal{B}_{ij}\mathcal{B}_{ij} \rangle} \tag{33}$$

where we assumed $\langle cfg \rangle \approx c\langle fg \rangle$ and $\langle \cdot \rangle$ denotes averaging over homogeneous directions. This general formulation is readily specified for the case $a_{ij} = m_{ij}^B$ and $b_{ij} = -\Delta^2 |S| S_{ij}$. In order to prevent numerical instability caused by negative values of the eddy-viscosity, the dynamic coefficient is set to zero wherever (33) returns negative values. This is referred to as 'clipping'. For further details we refer to [12].

The mathematical regularization of the Navier-Stokes equations which we pursue here involves a direct and explicit alteration of the nonlinear convective terms. In the context of this paper, this provides a systematic framework for *deriving* a subgrid model which is in sharp contrast with traditional phenomenological subgrid modeling. Several basic regularization principles have been proposed, e.g., the NS-α model based on maintaining a filtered Kelvin circulation theorem [3, 4, 20], or the Leray formulation [21] to which we will restrict in this paper.

In Leray regularization, one alters the convective fluxes into $\overline{u}_j \partial_j u_i$, i.e., the solution $\mathbf{u}$ is convected with a smoothed velocity $\overline{\mathbf{u}}$. Consequently, the nonlinear effects are reduced by an amount governed by the smoothing properties of the filter operation, L. The governing Leray equations are [21]

$$\partial_j \overline{u}_j = 0 \quad ; \quad \partial_t u_i + \overline{u}_j \partial_j u_i + \partial_i p - \frac{1}{Re}\Delta u_i = 0 \tag{34}$$

Leray solutions possess global existence and uniqueness with proper smoothness and boundedness, whose demonstration depends on the balance equation for $\int |\mathbf{u}|^2 \, d^3x$. Based on the Leray equations (34) we may eliminate $\mathbf{u}$ by assuming $\overline{\mathbf{u}} = L(\mathbf{u})$ and $\mathbf{u} = L^{-1}(\overline{\mathbf{u}})$. For convolution filters one has, e.g., $\partial_t u_i = \partial_t(L^{-1}(\overline{u}_i)) = L^{-1}(\partial_t \overline{u}_i)$ and the nonlinear terms can be written as $\overline{u}_j \partial_j(u_i) = \partial_j(\overline{u}_j u_i) = \partial_j(\overline{u}_j L^{-1}(\overline{u}_i))$. Consequently, one may readily obtain:

$$L^{-1}\Big(\partial_t \overline{u}_i + \partial_j(\overline{u}_j \overline{u}_i) + \partial_i \overline{p} - \frac{1}{Re}\Delta \overline{u}_i\Big) = -\partial_j\Big(\overline{u}_j L^{-1}(\overline{u}_i) - L^{-1}(\overline{u}_j \overline{u}_i)\Big) \tag{35}$$

This may be recast in terms of the LES template as:

$$\partial_t \overline{u}_i + \partial_j(\overline{u}_j \overline{u}_i) + \partial_i \overline{p} - \frac{1}{Re}\Delta \overline{u}_i = -\partial_j\Big(m_{ij}^L\Big) \tag{36}$$

The implied asymmetric Leray model m_{ij}^L involves both L and its inverse and may be expressed as:

$$m_{ij}^L = L\Big(\overline{u}_j L^{-1}(\overline{u}_i)\Big) - \overline{u}_j\overline{u}_i = \overline{\overline{u}_j u_i} - \overline{u}_j\overline{u}_i \tag{37}$$

The reconstructed solution u_i can in principle be found from any formal or approximate inversion L^{-1}. For this purpose one may use a number of methods, e.g., polynomial inversion [7], geometric series expansions [22] or exact numerical inversion of Simpson top-hat filtering [8] to which we return momentarily.

Similar to the turbulent stress tensor, the velocity-species stress tensor requires a closure model. Typically an eddy-diffusivity type formulation is adopted in literature in which $\zeta_{kj} \sim \partial_j\overline{c}_k$. Alternatively, the Leray regularization can be adopted also for ζ_{kj} leading to

$$\zeta_{kj} = L\Big(\overline{u}_j L^{-1}(\overline{c}_k)\Big) - \overline{u}_j\overline{c}_k = \overline{\overline{u}_j c_k} - \overline{u}_j\overline{c}_k \tag{38}$$

An extension to compressible flow is quite straightforward and will not be described further here. Rather, we turn to the filter inversion that is required for the Leray model. We will also adopt this to determine an explicit closure model for the chemical source terms.

3.2 Filter inversion and source-term modeling

The source term in the combustion model depends nonlinearly on the state-vector. Various models can be proposed for the source-term in the large-eddy context. Here, we will compare a model in terms of the filtered state vector with a model in which a partial inversion of the filter is adopted. For simplicity we focus on the stylized chemical reaction $F + O \rightarrow P$ introduced in the previous section. In this case only three species occur in a single chemical reaction and effectively only the filtered chemical source term $\overline{\omega}_1$ needs to be explicitly approximated. Once this source term is available we have $\overline{\omega}_2 = \alpha\overline{\omega}_1$, $\overline{\omega}_3 = -(1+\alpha)\overline{\omega}_1$ and $\overline{h_k\omega_k} = Q\overline{\omega}_1$.

The first model for the filtered source term uses an approximation in terms of the filtered state-vector:

$$\overline{\omega}_1 = -Da_O\overline{(\rho c_F)(\rho c_O)\exp(-\frac{Ze}{T})} \approx -Da_O(\overline{\rho}\widetilde{c}_F)(\overline{\rho}\widetilde{c}_O)\exp(-\frac{Ze}{\widetilde{T}}) \tag{39}$$

This model can be expected to capture the main dynamic contributions in cases where the filter-width Δ is quite small. Although this may not be the most challenging test for a large-eddy modeling, it does constitute a valuable point of reference.

The second model for $\overline{\omega}_1$ arises by invoking an approximation of the inversion of the spatial filter. In this case we arrive at a computational modeling in which

$$\overline{\omega}_1 \approx -Da_O\overline{(\rho^* c_F^+)(\rho^* c_O^+)\exp(-\frac{Ze}{T^+})} \tag{40}$$

Here $\rho^* = L^{-1}(\overline{\rho})$ and $f^+ = L_\rho^{-1}(\widetilde{f})$ in which L_ρ^{-1} denotes the approximate inverse of the Favre filter associated with L. The latter operator is applied to reconstruct some of the fine-scale structure in c_F, c_O and the temperature T. The evaluation of L_ρ^{-1} can readily be expressed in terms of L^{-1}. In fact, by definition of the Favre filter we have $L(\rho f) = L(\rho)L_\rho(f)$. Application of L^{-1} to this definition yields

$$L^{-1}\Big(L(\rho f)\Big) = \rho f = L^{-1}\Big(\overline{\rho}\widetilde{f}\Big) \tag{41}$$

From this relation we may isolate the unfiltered field f as

$$f = \frac{\rho f}{\rho} = \frac{L^{-1}\Big(\overline{\rho}\widetilde{f}\Big)}{L^{-1}(\overline{\rho})} \equiv L_\rho^{-1}(\widetilde{f}) \tag{42}$$

which defines the inversion of the Favre filter. Given $\widetilde{f}$ and $\overline{\rho}$ the inversion L_ρ^{-1} can be directly computed, provided the approximate inverse L^{-1} is available. The inversion L_ρ^{-1} can be applied to determine c_F^+, c_O^+ and T^+ that are required in this second model for $\overline{\omega}_1$.

There are various inversion procedures that may be adopted to approximate the inverse L^{-1}. A procedure that may be applied to general graded filters such as the top-hat or Gaussian filters arises from an expansion of L^{-1} in terms of a geometric series [22]:

$$L^{-1}(\overline{f}) = \Big(I-(I-L)\Big)^{-1}(\overline{f}) = \sum_{n=0}^{\infty}(I-L)^n(\overline{f}) \approx \sum_{n=0}^{N}(I-L)^n(\overline{f}) \equiv L_N^{-1}(\overline{f}) \tag{43}$$

Approximating the geometric series with $N+1$ terms we find the following computational inversion procedures:

$$\begin{array}{lll} N=0: & u^* = & L_0^{-1}(\overline{u}) = \overline{u} \\ N=1: & u^* = & L_1^{-1}(\overline{u}) = \overline{u} + (I-L)\overline{u} = 2\overline{u} - \overline{\overline{u}} \\ N=2: & u^* = & L_2^{-1}(\overline{u}) = \overline{u} + (I-L)\overline{u} + (I-L)(I-L)\overline{u} = 3\overline{u} - 3\overline{\overline{u}} + \overline{\overline{\overline{u}}} \end{array} \tag{44}$$

This method of approximate filter-inversion requires several applications of L, particularly in case of higher order inversion. Convergence toward the exact inverse is fastest in case the Fourier-transform of the filter-kernel is nowhere close to 0.

An alternative inversion procedure arises from the exact inversion of a particular numerical filter [8]. In one dimension numerical convolution filtering corresponds to kernels

$$G(z) = \sum a_j \delta(z - z_j) \quad ; \quad |z_j| \leq \Delta/2 \tag{45}$$

In particular, we consider three-point filters with $a_0 = 1-\alpha$, $a_1 = a_{-1} = \alpha/2$ and $z_0 = 0$, $z_1 = -z_{-1} = \Delta/2$. Here we use $\alpha = 1/3$ which corresponds to Simpson quadrature of the top-hat filter. In actual simulations the resolved fields are known only on a set of grid

points $\{x_m\}_{m=0}^N$. The application of L^{-1} to a general discrete solution $\{\overline{u}(x_m)\}$ can be specified using discrete Fourier transformation as [8]

$$L^{-1}(\overline{u}_m) = \sum_{j=-n}^{n} \Big(\frac{\alpha - 1 + \sqrt{1-2\alpha}}{\alpha} \Big)^{|j|} \frac{\overline{u}_{m+rj/2}}{(1-2\alpha)^{1/2}} \tag{46}$$

where the subgrid resolution $r = \Delta/h$ is assumed to be even. An accurate and efficient inversion can be obtained with only a few terms, recovering the original signal to within machine accuracy with $n \approx 10$. The sensitivity of the results to the inversion-accuracy was investigated and found not to be very critical.

The large-eddy simulations have been started from a suitably filtered initial condition as follows. In a first step a 256^3 representation of an initial condition for direct numerical simulations was generated. To obtain an initial condition for the large-eddy simulations, this field was filtered using the three-point Simpson quadrature approximation to the top-hat filter. The filter-width Δ was chosen identical to the filter-width that was selected for the subsequent large-eddy simulation. Throughout, we will adopt $\Delta = \ell/16$ [4]. In a second step the filtered data were restricted to the numerical grid of step-size Δx employed in the large-eddy simulations. Typical resolutions of 32^3, 64^3 and 96^3 were used, thereby covering the filter-width Δ by 2, 4 or 6 grid-cells respectively [23].

In the following two sections we will investigate to what extent the closures of the turbulent stress tensor and the approximate closure of the chemical source terms contribute to accurate large-eddy simulation of diffusion flames. First, in section 4 we turn to alterations in the properties of the developing turbulent flow and in section 5 we focus on the consequences for the flame properties.

4 Combustion-modulated turbulence

In this section we investigate three central flow-properties associated with the combustion process in a transitional and turbulent temporal mixing layer. We will consider the decay of the resolved kinetic energy E, the growth of the momentum-thickness δ and the spectral distribution of the energy $\mathcal{E}(k)$ in the turbulent regime. Specifically,

$$E(t) = \int_\Omega \frac{1}{2} \overline{u}_i \overline{u}_i \; d\mathbf{x} \quad ; \quad \delta(t) = \frac{1}{4} \int_{-\ell/2}^{\ell/2} \Big(1 - \langle \overline{u}_1 \rangle (x_2,t) \Big) \Big(\langle \overline{u}_1 \rangle (x_2,t) + 1 \Big) dx_2 \tag{47}$$

where Ω is the flow domain and $\langle \cdot \rangle$ denotes averaging over the homogeneous x_1 and x_3 directions. The evolution of E illustrates the transitional flow and subsequent self-similar decay in the turbulent regime. It depends primarily on the larger scales in the flow. Similarly, the momentum thickness is a large-scale quantity that can be used as a measure for the progress of the mixing while the kinetic energy spectrum characterizes the prediction of both the large and the small scales in the flow. We focus on the influence of the heat-release parameter Q on the turbulent flow.

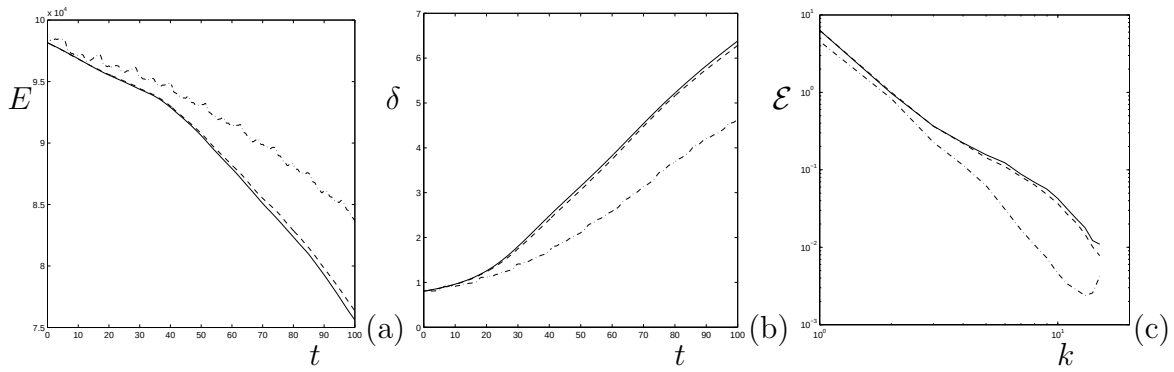

Figure 2: Decay of kinetic energy E (a), growth of momentum thickness δ (b) and kinetic energy spectrum $\mathcal{E}$ at a characteristic turbulent stage $t = 100$ (c). The resolution is 32^3 at $\Delta = \ell/16$ displaying the effect of the heat-release at $Q = -1$ (solid), $Q = -10$ (dashed), $Q = -100$ (dash-dotted).

In figure 2 we collected predictions obtained with the Leray regularization model for the turbulent stresses and inverse modeling of the chemical source terms. We observe a close similarity between predictions at $Q = -1$ and $Q = -10$, while a value $Q = -100$ leads to significant alterations compared to the no-combustion case. The decay of the kinetic energy is considerably reduced as the heat-release of the chemical process is increased (Fig. 2(a)). Moreover, a characteristic non-monotonous decay arises. We observe a strongly reduced mixing-rate at $Q = -100$ (Fig. 2(b)). This illustrates a remarkable competition in which the combustion process that actually requires mixing of fuel and oxidizer itself restricts this mixing. The effect is particularly strong for the small scales, as is clarified by the kinetic energy spectrum in the turbulent regime (Fig. 2(c)). The intense heat-release decreases the importance of the small scales in the turbulent flow which will affect localized wrinkling of the flame to which we turn in the next section.

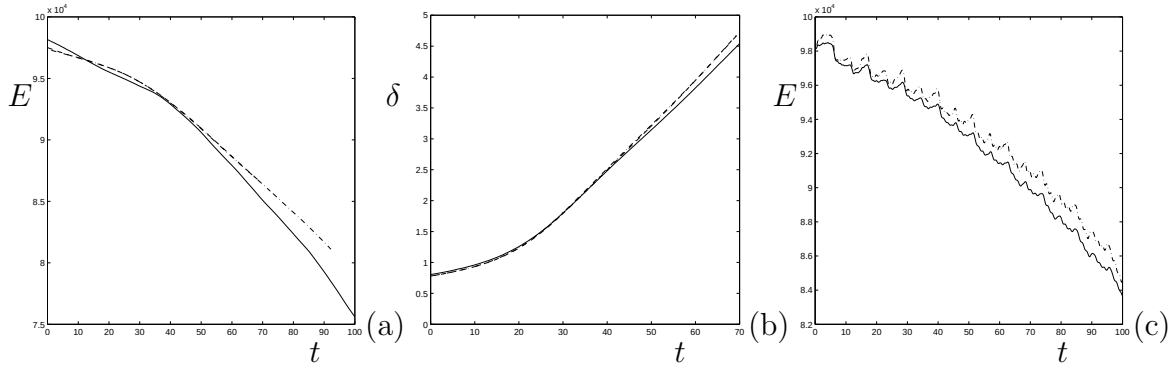

Figure 3: Convergence of Leray predictions for the kinetic energy E (a) and the momentum thickness δ (b) at $Q = -1$, $\Delta = \ell/16$ and resolution N^3 with $N = 32$ (solid), $N = 64$ (dashed) and $N = 96$ (dash-dotted). The effect of the combustion model is displayed in (c) at $Q = -100$ and $N = 32$: inverse modeling of source term (solid), mean flow model (dash-dotted).

The Leray predictions at a resolution 32^3 correspond to a subgrid resolution $r = \Delta/(\Delta x) = 2$. The influence of the numerical discretization on these results is illustrated in figure 3(a,b). We observe that the kinetic energy and momentum thickness are well approximated at this subgrid resolution, while an increase in r to a value of 4-6 is seen to closely correspond to the grid-independent large-eddy prediction for the Leray model [23, 24]. The dependence of the predictions on the combustion model is displayed in figure 3(c). The reconstructed small-scale features of the large-eddy solution that are used in the inverse modeling of the chemical source terms are seen to lead to a slightly stronger decay of the kinetic energy. The influence of this combustion model on the momentum thickness was found to of comparable relative magnitude while the kinetic energy spectrum displayed some differences primarily in the smallest resolved scales. The application of inverse filtering at very low resolution and strong combusion needs to be further investigated. This addresses specifically reaction zones that are very much smaller than the gridsize of the large-eddy simulation which form a significant challenge to this type of modeling.

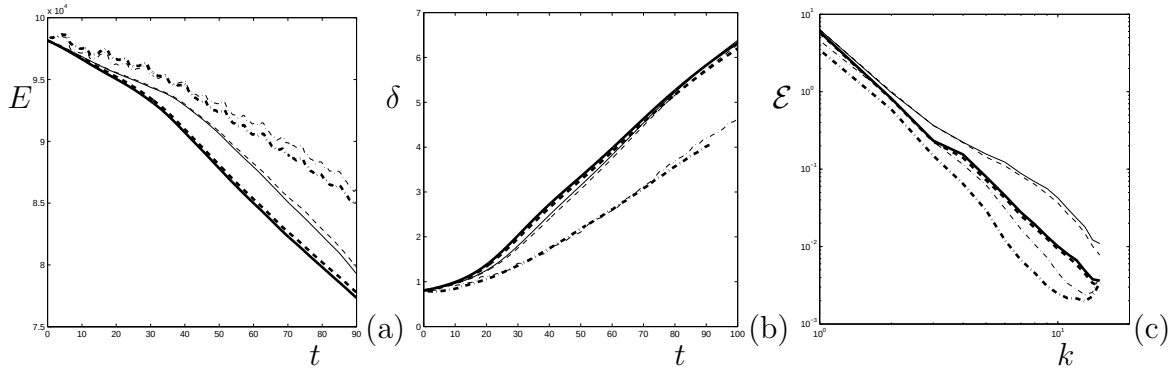

Figure 4: Comparison of Leray (thin lines) and dynamic mixed model (thick lines) predictions. Decay of kinetic energy E (a), growth of momentum thickness δ (b) and kinetic energy spectrum $\mathcal{E}$ at a characteristic turbulent stage $t = 100$ (c). The resolution is 32^3 at $\Delta = \ell/16$ displaying the effect of the heat-release at $Q = -1$ (solid), $Q = -10$ (dashed), $Q = -100$ (dash-dotted).

The results obtained by using the dynamic mixed subgrid model are compared with the Leray results in figure 4. We observe that the decay of the kinetic energy is more pronounced when use is made of the dynamic mixed model. This difference has hardly any influence on the prediction of the momentum thickness, while the small scales in the large-eddy solution are strongly reduced in case the dynamic mixed model is adopted. These differences in the large-eddy predictions affect the prediction of properties of the combustion process. We will turn to this in the next section.

5 Level-set analysis of turbulent flame properties

To quantify basic properties of an evolving diffusion flame we concentrate on 'global' variables, such as the flame-area and the wrinkling of the flame. The flame itself is defined by the level-set $S(t)$ where the 'level-function' $F(\mathbf{x},t) = c_F(\mathbf{x},t) - c_O(\mathbf{x},t) = 0$. In general, the global variable corresponding to a so-called 'density function' f is defined as

$$\mathcal{F}(t) = \int_{S(t)} dA\ f(\mathbf{x},t) = \int_{\Omega} d\mathbf{x}\ \delta(F(\mathbf{x},t))|\nabla F(\mathbf{x},t)| f(\mathbf{x},t) \tag{48}$$

where the flow-domain Ω encloses the level-set $S(t)$. The formulation in (48) was used as the basis of the numerical quadrature method that was developed in [10]. To determine the surface-area A of the flame we adopt $f_A = 1$. A measure for the global 'curvature' C is obtained using as density

$$f_C(\mathbf{x},t) = \nabla \cdot \mathbf{n} \quad ; \quad \mathbf{n}(\mathbf{x},t) = \frac{\nabla F(\mathbf{x},t)}{|\nabla F(\mathbf{x},t)|} \tag{49}$$

where $\mathbf{n}$ denotes the unit normal on the flame surface. The 'wrinkling' W is obtained using $f_W(\mathbf{x},t) = |\nabla \cdot \mathbf{n}|$.

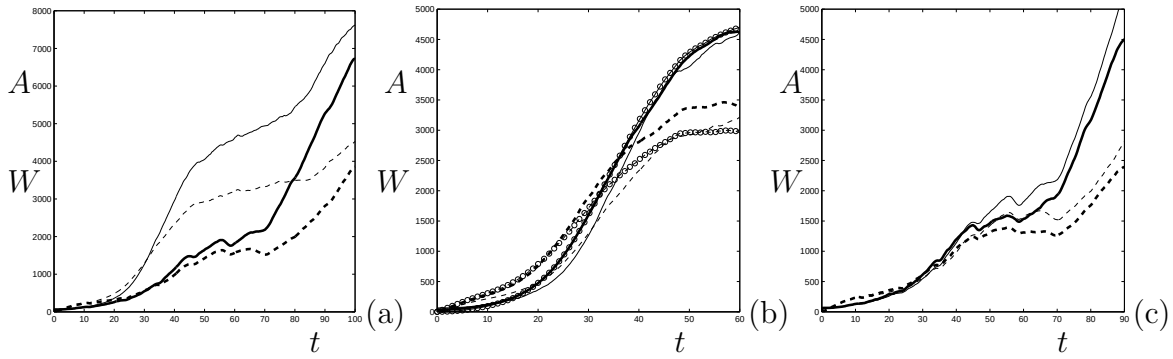

Figure 5: Evolution of the flame area $A(t) - A(0)$ (solid) and wrinkling W (dashed) (a) as predicted by the Leray regularization model at $Q = -1$ (thin lines) and $Q = -100$ (thick lines) using a resolution of 32^3, (b) convergence of Leray predictions of $A(t) - A(0)$ (solid) and W (dashed) at $Q = -1$ and resolution N^3 with $N = 32$ (thin lines), $N = 64$ (thick lines) and $N = 96$ (thin lines with $\circ$) and (c) evolution of the flame area $A(t) - A(0)$ (solid) and wrinkling W (dashed) at $Q = -100$ as predicted by the Leray regularization model (thin lines) and the dynamic mixed model (thick lines) using a resolution of 32^3.

In figure 5(a) we show the development of the flame's surface-area A and its total wrinkling W obtained at different values for the heat-release parameter. We adopted inverse modeling for the chemical source terms. The growth of the area and wrinkling follows the general scenario that occurs in this mixing layer as mentioned in subsection 2.2. In case the heat-release is modest, i.e., at $Q = -1$, we notice a marked increase of the area and wrinkling between $t = 30 - 40$ and between $t = 80 - 100$, corresponding to the

pairing of streamwise vortices (see also [11]). At much stronger heat-release $Q = -100$ we notice that both the area and wrinkling are considerably lower, consistent with the observed 'calming' of the mixing process under these conditions, cf. figure 2.

At a coarse spatial resolution the results are to some degree influenced by the numerical method. This effect is quite small for the developing flame-area and wrinkling as illustrated in figure 5(b) where we compare Leray predictions at subgrid resolutions $r = 2, 4$ and 6. The general behavior is quite well captured at $r = 2$. The approximately grid-independent solution appears to be obtained for the flame-area at $r = 4-6$ while the small-scale properties expressed in the wrinkling of the flame are somewhat more sensitive to the numerical representation.

The effect of the subgrid model for the turbulent stress tensor on the flame-properties is quantified in figure 5(c). The Leray model was shown to retain more of the small-scale variability in the large-eddy solution (cf. figure 4). This translates into slightly higher values for the flame-area and wrinkling when compared to the dynamic mixed model results. At the selected Schmidt number $Sc = 10$ this effect is not very pronounced, but it may be expected that at higher Sc the differences will be increased.

Motivated by the interpretation of the stoichiometric surface, we may introduce a 'thick' active flame region around this surface, defined by $D(a) = \{\mathbf{x} \in \mathbb{R}^3 |\ |c_F - c_O| \leq a\}$ in which the parameter a is referred to as the 'stoichiometric width'. The fuel conversion-rate Γ_F associated with $D(a)$ is defined by

$$\Gamma_F(a,t) = \int_{-a}^{a} ds \int_{c_F - c_O = s} dA\ \omega_F(\mathbf{x},t) \tag{50}$$

The conversion rate Γ_F arises mainly from the region in physical space close to the flame-surface. When the width a increases Γ_F increases as well with a maximum at $a = 1$, in which case all chemical conversion in the entire flow-domain is included. The introduction of the fuel conversion-rate Γ_F allows to define the ε-flame-region by $\Gamma_F(a,t)/\Gamma_F(1,t) = \varepsilon$ from which the value of $a(\varepsilon,t)$ may be solved. In this way it becomes possible to quantify the region around the flame-surface in which a fraction ε of the total conversion-rate occurs.

In figure 6 we collected the evolution of the stoichiometric width a as obtained with the Leray regularization model. We considered the region where about 25 %, 50 % or 75 % of the total conversion-rate occurs. After the transitional stages a fairly constant value of a defines the active flame region. In particular, we notice that a value of about $a \approx 0.16$ yields 25 %, $a \approx 0.36$ yields 50 % and $a \approx 0.6$ corresponds to 75 % of the total conversion-rate. It is interesting to observe that the value of the heat-release parameter Q does not have a significant influence on the stoichiometric width. This seems to indicate a degree of 'similarity' in the developing flames, which will be further investigated in the future. The physical space region that contains the active part of the flame increases with time as the flow goes through a transition to turbulence. This is shown in figure 7, displaying a highly distorted flame. The indicated region contains the level-sets $|c_F - c_O| \leq a$ for

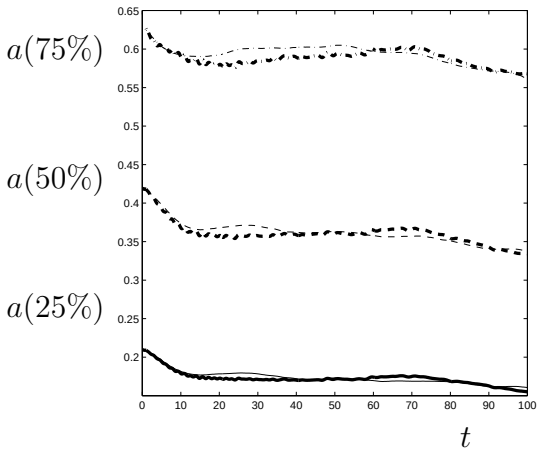

Figure 6: Stoichiometric width a corresponding to 75 % (top, dash-dotted), 50 % (middle, dashed) and 25 % (bottom, solid) of the total conversion rate at $Q = -1$ (thin lines) and $Q = -100$ (thick lines) using a resolution of 32^3.

$|a| \leq 0.35$.

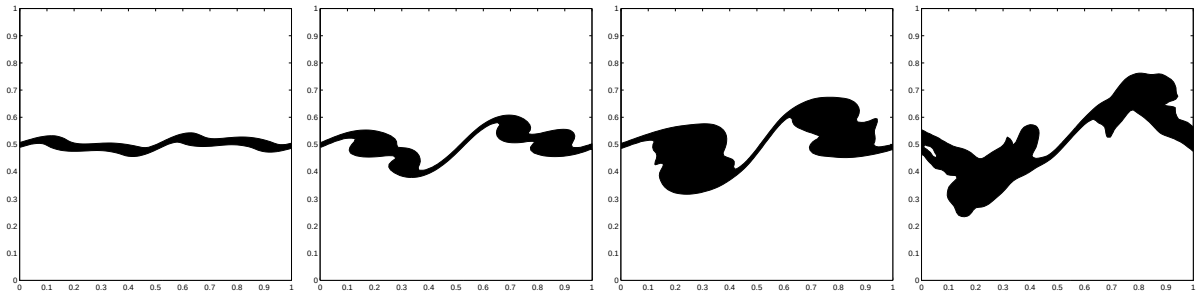

Figure 7: Active flame region in which 50% of the total conversion occurs, at $Q = -10$. A characteristic slice is shown at $t = 15, 35, 55, 75$ (from left to right).

6 Concluding remarks

In this paper, we introduced a simple combustion model and studied a turbulent diffusion flame in a temporal mixing layer. The coupling between the combustion and the turbulent transport induces a significant modulation of the turbulent flow properties, e.g., characterized by a strongly reduced spreading rate of the mixing layer. The dynamic mixed model was compared to the Leray regularization model for the turbulent stress tensor in large-eddy simulation. Moreover, a mean-flow parameterization of the filtered chemical source terms was confronted with a formulation based on approximate inversion. At the combustion - and flow-conditions studied here, the dependence of the predictions on the source-term modeling is quite limited. Likewise, the influence of the subgrid model is not very pronounced, which is all the more remarkable in view of the differences be-

tween these models and the fact that a coarse-grid simulation without any subgrid model yields significant differences. Evidently, the dynamic effects of the small scales in the flow are quite important and also well represented by either of the subgrid models.

Using a numerical method for integration over geometrically complex evolving level-sets, basic properties such as flame-area, wrinkling and active flame region were quantified. It was shown that these geometrical flame properties follow the basic scenario of the developing mixing layer. The two periods in which pairing of streamwise vortices dominated the flow were found to coincide with periods of increased growth of the flame-area and wrinkling. These global properties of the flame could be robustly predicted with the Leray and dynamic mixed models. A significant decrease of area and wrinkling was found to occur in case the heat-release became dynamically more important.

The findings of this paper indicate that large-eddy simulation based on either the Leray or the dynamic mixed subgrid models yields qualitatively similar results. The Leray model appears to retain more of the small-scale variability in the flow which influences quantitatively a number of flow and combustion characteristics. The dynamic mixed subgrid model was found to be among the more accurate models describing turbulent mixing [11]. Here we find largely comparable results based on the Leray model (see also [4]). However, compared to the intuitive modeling of the dynamic mixed model, the regularization principle that underlies the Leray formulation is much more transparent from a physics point of view. This is a main advantage that arises by starting from 'first principles' and is essential in case extension toward more complex situations is concerned. The regularization modeling that arises from the Lagrangian averaged Navier-Stokes framework [20] was found to be more accurate than the Leray model for turbulent mixing without combustion. Its extension to flows with combustion is subject of ongoing research and will be published elsewhere.

Acknowledgment

The author would like to acknowledge fruitful discussions with Philip de Goey, Rob Bastiaans and Jeroen van Oijen of the Combustion Technology Group at Eindhoven University of Technology.

REFERENCES

[1] Peters, N.: 2000. *Turbulent combustion*. Cambridge University Press. Cambridge.

[2] Geurts, B.J.: 2005. Iso-surface analysis of a turbulent diffusion flame, Proceedings ECMI-2004, Springer Verlag, 222-228, ISBN: 3-540-28072-3

[3] Geurts, B.J., Holm, D.D.: 2003. Regularization modeling for large-eddy simulation. *Phys. of Fluids*, **15**, L13

[4] Geurts, B.J., Holm, D.D.: 2006. Leray and NS-α modeling of turbulent mixing, *J. of Turbulence*, **7** (10), 1 - 33.

[5] Zang, Y., Street, R.L., Koseff, J.R.: 1993. A dynamic mixed subgrid-scale model and its application to turbulent recirculating flows. *Phys. of Fluids A*, **5**, 3186.

[6] Vreman, A.W., Geurts, B.J., Kuerten, J.G.M.: 1994. On the formulation of the dynamic mixed subgrid-scale model. *Phys. of Fluids* **6**, 4057

[7] Geurts, B.J.: 1997. Inverse Modeling for Large-Eddy Simulation. *Phys. of Fluids* **9**, 3585

[8] Kuerten, J.G.M., Geurts, B.J., Vreman, A.W., Germano, M.: 1999. Dynamic inverse modeling and its testing in large-eddy simulations of the mixing layer. *Phys. of Fluids* **11**, 3778-3785

[9] Pope, S.B.: 2000. *Turbulent Flows*. Cambridge University Press. Cambridge.

[10] Geurts, B.J.: 2001. Mixing efficiency in turbulent shear layers. *J. of Turb.* **2**:17.

[11] Vreman, A.W., Geurts, B.J., Kuerten, J.G.M.: 1997. Large-eddy simulation of the turbulent mixing layer. *J. Fluid Mech.*, **339**, 357.

[12] Geurts B.J.: 2003. Elements of Direct and Large-Eddy Simulation. Edwards Publishing. ISBN: 1-930217-07-2.

[13] Bastiaans, R.J.M., Somers, L.M.T., de Lange, H.C.: 2001. DNS of non-premixed combustion in a compressible mixing layer. In: Modern strategies for turbulent flow simulation. Ed.: B.J. Geurts, R.T. Edwards Publishers, Philadelphia.

[14] Vreman, A.W., Geurts, B.J., Kuerten, J.G.M.: 1995. Subgrid-modeling in LES of compressible flow. *Applied Scientific Research*, **54**, 191.

[15] Bardina, J., Ferziger, J.H., Reynolds, W.C.: 1984. Improved turbulence models based on LES of homogeneous incompressible turbulent flows. Department of Mechanical Engineering. *Report No. TF-19*, Stanford.

[16] Smagorinsky, J.: 1963. General circulation experiments with the primitive equations. *Mon. Weather Rev.*, **91**, 99.

[17] Germano, M., Piomelli U., Moin P., Cabot W.H.: 1991. A dynamic subgrid-scale eddy viscosity model. *Phys.of Fluids*, **3**, 1760.

[18] Germano, M.: 1992. Turbulence: the filtering approach. *J. Fluid Mech.*, **238**, 325.

[19] Lilly, D.K.: 1992. A proposed modification of the Germano subgrid-scale closure method. *Phys. of Fluids A*, **4**, 633.

[20] Foias, C., Holm, D.D., Titi, E.S.: 2001. The Navier-Stokes-alpha model of fluid turbulence. *Physica D*, **152**, 505.

[21] Leray, J.: 1934. Sur les movements d'un fluide visqueux remplaissant l'espace. *Acta Mathematica*, **63**, 193.

[22] Stolz, S., Adams, N.A.: 1999. An approximate deconvolution procedure for large-eddy simulation. *Phys. of Fluids*, **11**, 1699.

[23] Geurts, B.J., Fröhlich, J.: 2002. A framework for predicting accuracy limitations in large-eddy simulation. *Phys. of fluids*, **14**, L41.

[24] Meyers, J., Geurts, B.J., Baelmans, M.: 2003. Database-analysis of errors in large-eddy simulations. *Phys. Fluids* **15**, 2740.